Parameterisation of Respiratory Impedance in Lung Cancer Patients From Forced Oscillation Lung Function Test

Maria Ghita , *Member, IEEE*, Charlotte Billiet, Dana Copot , *Member, IEEE*, Dirk Verellen, and Clara M. Ionescu , *Senior Member, IEEE*

Abstract—*Objective:* **This study aims to analyze the contribution and application of forced oscillation technique (FOT) devices in lung cancer assessment. Two devices and corresponding methods can be feasible to distinguish among various degrees of lung tissue heterogeneity.** *Methods:* **The outcome respiratory impedance Z_{rs} (in terms of resistance R_{rs} and reactance X_{rs}) is calculated for FOT and is interpreted in physiological terms by being fitted with a fractional-order impedance mathematical model (FOIM). The non-parametric data obtained from the measured signals of pressure and flow is correlated with an analogous electrical model to the respiratory system resistance, compliance, and elastance. The mechanical properties of the lung can be captured through G_r to define the damping properties and H_r to describe the elastance of the lung tissue, their ratio representing tissue heterogeneity η_r.** *Results:* **We validated our hypotheses and methods in 17 lung cancer patients where we showed that FOT is suitable for non-invasively measuring their respiratory impedance. FOIM models are efficient in capturing frequency-dependent impedance value variations. Increased heterogeneity and structural changes in the lungs have been observed. The results present inter- and intra-patient variability for the performed measurements.** *Conclusion:* **The proposed methods and assessment of the respiratory impedance with FOT have been demonstrated useful for characterizing mechanical properties in lung cancer patients.** *Significance:* **This correlation analysis between the measured clinical data motivates the use of the FOT devices in lung cancer patients for diagnosis of lung properties and follow-up of the respiratory function modified due to the applied radiotherapy treatment.**

Index Terms—**Bioimpedance, forced oscillation technique, fractional order impedance model, identification, lung cancer, mathematical modeling, obstructive disease, respiratory biomechanics, tissue heterogeneity.**

Maria Ghita is with the Research Group of Dynamical Systems and Control, Ghent University, 9052 Ghent, Belgium, also with the Faculty of Medicine and Health Sciences, Antwerp University, 2610 Wilrijk, Belgium, and also with the EEDT – Core Lab on Decision and Control, Flanders Make Consortium, and also with the Cancer Research Institute Ghent, 9052 Ghent, Belgium (e-mail: maria.ghita@ugent.be).

Charlotte Billiet and Dirk Verellen are with the Department of Radiation Oncology, Iridium Network – GZA Hospital, Sint-Augustinus, and also with the Department of Radiotherapy, Faculty of Medicine and Health Sciences, Antwerp University, Belgium.

Dana Copot and Clara M. Ionescu are with the Research Group of Dynamical Systems and Control, Ghent University, Belgium, and also with the EEDT – Core Lab on Decision and Control, Flanders Make Consortium, Belgium.

I. INTRODUCTION

EVIDENCE suggests that patients diagnosed with lung cancer, particularly non-small cell lung cancer (NSCLC), undergoing a pulmonary function test (PFT) during the clinical assessment may benefit from increased personalized treatment (e.g., accuracy, testing, prediction, etc.) [1]. The quantitative assessment of lung function is crucial to provide information, thereby supporting the decision-making process in treatment planning. This implies an evaluation of the lung function mechanics, albeit critically restricted by the pathology [2]. In patients with early-stage lung cancer having comorbidities or limited lung function, a lobectomy is not feasible. In these patients, stereotactic body radiation therapy (SBRT) is a valid and recommended treatment strategy [2].

The forced oscillation technique (FOT) is a noninvasive, non-standardized method for assessing respiratory impedance during tidal breathing [3], [4], [5]. FOT being maneuverless, becomes suitable in patients with breathing difficulties, infants, and non-cooperative patients [5]. Measuring lung function in patients with obstructive airways diseases has been proven useful in clinical practice [6] for smokers [7], patients with asthma [8], [9], COPD [8], [10], [11], [12], [13], [14], cystic fibrosis [15], kyphoscoliosis [16], airway abnormalities and interstitial pneumonia [17] or obstructive sleep apnea [18], as well as in patients that underwent general anesthesia and received oxygen supply [19]. Evidence suggests that lung function mechanics may change in NSCLC patients [1]. In these frail patients, we expect that FOT will play a pivotal role in addressing lung function as a routine assessment for lung cancer management.

Airflow obstruction is a surrogate marker of carcinogenic presence in the airways. Medium and small size airways dysfunction as evaluated by FOT are associated with the fluctuation of the heterogeneity of airway constriction over time [20]. The tumor location influences the obstruction's location (already partially affected by asthma or COPD in some patients), which

results in a considerable increase of heterogeneity in the tissue, airways disruption, and lung failure [21]. This marker of inhomogeneities has an influence on the overall mechanical properties of the lung. However, the precise nature and level of this heterogeneity are difficult to ascertain. Tissue heterogeneity (hysteresivity) is described by Bates in [22] as the ratio between resistance and elastance of lung tissue, further accounting for tissue impedance [23].

Lung function mechanics are assessed by FOT in their frequency response representation as a result of excitatory oscillations at various frequencies [3], [24]. This information is known as respiratory impedance, a complex variable, whereas the real part is known to characterize the total resistance, and the imaginary part is the balance between inertive and compliant (reactance) mechanical properties [25]. Resistance and reactance of the respiratory system are correlated with morphological changes in the lungs, represented by mechanical properties at 4–50 Hz frequency interval [6], [20]. Tissues with tumorous cells will induce heterogeneity in dynamic response, tissue viscoelasticity, and tissue damping [22], [26]. Various mechanics are assessed at different frequency ranges. Viscoelasticity may be evaluated at lower frequencies, encompassing spontaneous breathing rates (<2 Hz) [5], [10].

Parameterisation of respiratory frequency response is effectively and physiologically motivated by emerging mathematical models of non-integer orders into a fractional order impedance model (FOIM) [27]. FOIMs characterize successfully the dynamic mechanical behavior of lung tissues [8], [11], [27], [28] and electrical impedance.

Our study is the first to undertake an extensive analysis of respiratory impedance modeling in patients with lung cancer. Together with tissue heterogeneity characterization, measuring lung function with noninvasive FOT devices may prove to deliver complementary information for the decision-making process in measuring the effectiveness of the treatment applied to lung cancer. As such, fusion through parameterisation of multiple information sources (lung function tests, pretreatment evaluation, tumor volume images, etc.) in mathematical models, are core instruments in the path to optimality when radiotherapy and multi-drug therapies are envisaged. In clinical practice, SBRT can be delivered in lung tissue for early-stage lung cancer with a limited number of metastatic lesions in the lung [29]. This treatment has demonstrated high local control rates with limited toxicity. A very high dose is delivered very precisely with steep dose gradients in one or a few fractions to small target volumes, while controlling tumor movement [30]. Fractionation schedules are determined in function of tumor location inside the lungs (central/peripheral).

The objective of this study is to investigate the potential use of FOT in patients diagnosed with NSCLC, undergoing SBRT. A parameterisation is performed, from frequency response respiratory impedance data to FOIMs. This paper provides the first evidence for the correlation between lung function mechanics and FOIM values in patients with lung cancer.

The remainder of the paper is organized as follows. Section II introduces the study design, afferent clinical data, and measurement FOT devices, continuing with the processing methods of the clinical trial data set. The results and statistical analyses are
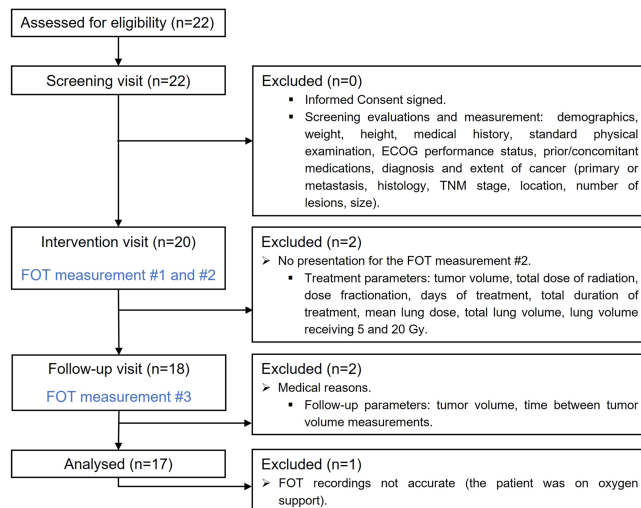

Fig. 1. Flow diagram for the study protocol performed at GZA hospital. The reported clinical data from the trial include all the subject numbers involved (enrolled, excluded, and analyzed).

presented in Section III. Finally, the scientific discussion is given in Section IV, followed by Conclusions.

II. MATERIALS AND METHODS

A. Data Collection

1) Study Design: The patient-specific data is collected from an interventional non-randomized clinical trial conducted at GasthuisZusters Hospital Sint-Augustinus in Antwerpen, Belgium ("Respiratory impedance models for noninvasive lung function testing in individualized stereotactic body radiation therapy (RIMIRT)"), protocol no. CTOR20105GZA, Eudamed no. CIV-BE-21-03-036104, FAGG reference no. 80M0881). This study was organized following approval from the Medical Ethics Committee GZA and conducted in accordance with the Declaration of Helsinki and applicable regulatory.

The present research explores, for the first time, whether lung impedance measured by the FOT device correlates with SBRT dose distributions for patients with NSCLC or lung metastases eligible for SBRT according to institutional guidelines. The patients enrolled in the interventional pilot study fulfilled all the inclusion criteria: male or female, aged 18 years or above, diagnosed with NSCLC or oligometastatic disease eligible for SBRT, having an Eastern Cooperative Oncology Group (ECOG) Performance Status grade 0–2. Each patient signed an informed consent form indicating that he/she understands the purpose and procedures required for the study and is willing to participate in the study and comply with all the requirements.

The protocol is summarized in Fig. 1. The data was recorded during three visits of the patients to the oncological center:

1) Screening visit: patient inclusion and recording of screening assessments,
2) Intervention visit: FOT measurement #1 performed on the day of SBRT treatment simulation and FOT measurement #2 done on the last day of RT administration),

3) Follow-up visit: FOT measurement #3 achieved during the standard follow-up visit of the patient, usually approx. 3 months after the last treatment day.

The measurement protocol consisted of evaluating the respiratory function of included patients with two FOT devices manipulated by the technician. The patients underwent the measuring procedures consisting of breathing normally through the mouthpiece of the device without occluding it, sitting in a straight position on a chair, wearing a nose clip, and supporting his/her cheeks with his hands during the measurements, to minimize dead space effects.

The lung function of each patient was evaluated with the following devices:

- A commercialized FOT device at high-range frequencies – Resmon PRO for 60 seconds.
- The prototype 4P-FOT device at low-range frequencies for 140 seconds.

Between the measurements, a 5 minutes break was considered to allow similar respiratory mechanics as initial conditions in both measurements.

Additional information was provided from computed tomography (CT) scans upon the tumor volume of each patient and monitored to assess tumor progression before and after the SBRT treatment, at the time of FOT measurements #1 and #3.

2) Patient-Specific Clinical Data: A total of 22 patients diagnosed with lung cancer have been enrolled in the study, with only 17 participants attending all the study visits for the FOT measurements. Following completion of the cancer treatment, 5 patients had to be excluded from the analyses due to their absence at the monitoring visits, clinical reasons, or inaccurate FOT recording. Primary clinical data of the patients relevant to this study are listed in Table I, while detailed patient demographics have been published in [31]. All patients underwent the medical recommendations of their SBRT treatment scheme. The tumor volume shrinkage and respiratory health parameters are reported for quantifying the severity of the disease in Table II.

B. Measurement Devices

Two FOT devices were used for the assessment of lung function: low-range frequencies (0.2–2 Hz) 4th generation prototype 4P-FOT device (developed by DySC Research Group, Ghent University, Ghent, Belgium) [32], [33] and high-range frequencies (5–37 Hz) Resmon PRO FULL FOT system (manufactured by ResTech, Milano, Italy, and distributed by MGC Diagnostics, Minnesota, USA) [34]. The two devices are depicted in Fig. 2.

The prototype 4P-FOT device at lower frequencies superimposes a multisine signal at frequencies closer to the breathing of the patient in the range of 0.2–2 Hz (i.e., 0.25, 0.35, 0.45, 0.65, 0.85, 0.95, 1.15, 1.25, 1.35, 1.55, 1.75, 1.85, 1.95 Hz), for a measurement time of 140 seconds [24], [32], [33]. During the procedure, the pressure and air-flow data are monitored, together with the digital timer. The respiratory impedance is calculated post-measurements using the processing algorithm given hereafter.

TABLE I
BIOMETRIC INFORMATION OF INCLUDED PATIENT POPULATION (N=17)

	Median	Interquartile range
Age (y)	61.16	(46-80)
BMI[a]	26.9	(19.6–33.8)
Follow-up time (days)	126.35	(63-191)
	n	% of the population
Sex		
Male	11	64.7%
Female	6	35.29%
TNM Classification of Malignant tumors[b]		
T0N0M1	8	47.05%
T1N0M0	7	41.17%
T2N0M0	2	11.76%
ECOG Performance Status[c]		
ECOG 0	6	35.29%
ECOG 1	10	58.82%
ECOG 2	1	5.88%
Smoking history		
Active	8	47.05%
Ex-smoker	4	23.52%
Never	5	29.41%
Respiratory disorders		
COPD GOLD2[d]	1	5.88%
COPD GOLD3	5	29.41%
COPD GOLD4	1	5.88%
Asthma	1	5.88%
Pneumonitis	1	5.88%
No respiratory disorder	8	47.05%
Medical history		
Previous lung surgeries	5	29.41%
Previous lung RT	2	11.76%
Tumor lesions number (n=20)		
1 (cm^3)	10	50%
$\geq$1 (cm^3)	10	50%

Abbreviations: [a]BMI = body mass index. [b]TNM stage is a globally recognized standard for classifying the anatomical extent of tumor cancers, classified at the time of RT treatment. T: size or direct extent of the primary tumor (T0: no evidence of tumor, T1, T2: size and/or extension of the primary tumor), N: degree of spread to regional lymph nodes (N0: no regional lymph nodes metastasis), M: presence of distant metastasis (M0: no distant metastasis, M1: metastasis to distant organs). [c] ECOG = Eastern Cooperative Oncology Group Performance Status: 0 – Asymptomatic, 1 – Symptomatic but completely ambulatory, 2 – Symptomatic, <50% in bed during the day. [d]COPD GOLD is the classification of airflow limitation severity in COPD, based on the Global Initiative for COPD guidelines.
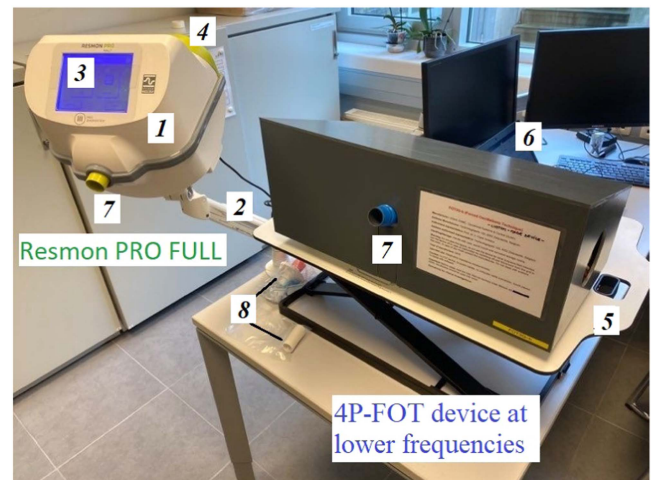

Fig. 2. Clinical set-up consisting of the two FOT devices. Resmon PRO is a standalone device with two parts: device *(1)* and an arm holder *(2)*. It is provided with a touchscreen display *(3)* to interact with the user and a USB port *(4)* to save the acquired data. The 4P-FOT device at lower frequencies is mounted on a height-adjustable table *(5)* and is connected to a laptop *(6)* with built-in programs and a user interface. For each measurement, single-use mouthpiece *(8)* is connected to slot *(7)*.

TABLE II
SUMMARY OF DISEASE SEVERITY PER PATIENT

Pat. ID	BMI	Sex	ECOG	Smoking history	Medical history	Lung volume (cm^3)	Mean lung dose (Gy)	TV (cm^3)	TV after RT (%)
P1	23.5	M	1	active	pneumonitis	4870.8	1.2	0.6	66.7%↓
P2	30.5	M	1	ex-smoker	NA	2653.7	2.7	0.9	100%↓
P3	26.2	F	1	active	COPD	3758.1	2.4	1	50%↓
P5	23.5	M	0	never	NA	5031.4	1.1	0.4	100%↓
P6	25.8	M	1	active	COPD GOLD 3	5263.3	2.1	4.2	66.7%↓
P8	33.8	M	2	active	COPD GOLD 3	3598.8	3.4	18	91.7%↓
P9	21.3	M	1	never	NA	5485.3	2.5	5.7	42.1%↓
P10	19.6	M	1	active	NA	3932.6	1.9	4.3	53.5%↓
P11	29.4	M	0	active	COPD GOLD 3	3340.5	5.3	5.4	48.1%↓
P12	29.7	F	0	never	NA	2335	7.3	1.2	33.3↑
								0.9	100%↓
								0.9	66.7↓
P13	23.7	F	0	never	NA	2886.4	5	0.9	55.6%↓
								5.6	17.9%↓
P14	29.4	M	1	ex-smoker	asthma	2229	3.7	2.6	100%↓
P15	24.9	F	1	active	COPD GOLD 2	3307.4	1	1.5	4.8%↑
P18	28.4	M	1	ex-smoker	COPD GOLD 3	4463.8	1	1.5	80%↓
P19	26.7	F	1	ex-smoker	COPD GOLD 4	3336.3	1.2	0.3	33.3%↓
P20	29.9	M	0	active	NA	2602.2	1.7	1.1	0%
								0.4	50%↑
P21	30.8	M	0	never	NA	2392.4	1.9	0.6	100%↓

Patients ID 4, 7, 16, 17, and 22 are missing from reported data due to clinical reasons. NA = not applicable.

A Pseudo Random Noise (PSRN) stimulating waveform is selected in Resmon PRO to measure the impedance at a frequency range of 5–37 Hz (i.e., 5, 7, 11, 13, 17, 19, 23, 29, 31, 37 Hz), for 60 seconds [34]. During the procedure, real-time tracking for volume and impedance at the lowest frequency 5 Hz (in the form of resistance and reactance) is displayed on the screen of the device. The remaining time to the end of the test is continuously reported on the screen. The results of the test can be reviewed on screen at the end of the measurement (graphical representation of resistance and reactance at the frequencies of the PSRN). Next, a clinical report for the specific patient is automatically exported by the investigator, together with all session data (archive with raw data of impedance values for each parameter). Being a commercial device, exported data of Resmon PRO involved the assessment of different parameters such as: measurement details (date and time of the sessions), mean (M) (with within-test coefficient of variation ($CV\%$)), Z-score, percentage of the predicted values ($\%pred$) and the predicted value ($pred$), mean total resistance (R_{rs} [cmH$_2$O/(l/s)]), mean total reactance (X_{rs} [cmH$_2$O/(l/s)]), resonant frequency (F_{res} [Hz]), index of heterogeneity of the obstruction within the lungs (R_{5-19}), duration of inspiration (T_i [s]), duration of expiration (T_e [s]), ratio between inspiratory time and total breath duration (T_i/T_{tot}), respiratory rate (RR [bpm]), tidal volume (V_t [l], mean inspiratory flow (V_t/T_i [l/s]), mean expiratory flow (V_t/T_e [l/s]), minute ventilation (V_e [l/min]) [34]. The values of the parameters are reported for each patient in Table IV.

Both devices and the measurements stop automatically after the predefined measurement time. Each device was calibrated before starting the measurement sessions with specific factory calibration objects according to international recommendations [5]. Further details regarding the devices' structure and calibration procedure are given in [24], [33], [34].

C. Data Processing in 4P-FOT Device

For the 4P-FOT device at low frequencies, the impedance is estimated based on the multisine excitation of 7 periods of 20.000 samples, sampled at 500 Hz frequency. The first period is excluded from the analysis to avoid breathing load transients. The excitatory signal is maintained at a peak-to-peak variation of around 0.2 kPa. Similarly, for Resmon PRO the first three breaths are not used for the calculation of impedance to allow for the amplitude of the stimulating waveform to be optimized according to the breathing pattern (i.e., excitatory signal not correlated to breathing harmonics). In contrast with 4P-FOT, Resmon PRO uses prediction equations for the determination of the individual normal range of respiratory parameters. The corresponding reference equations chosen for Resmon PRO analysis of the patients' group studied are those published in [36].

Respiratory physiology is determined by three fundamental parameters that describe the motion during the respiratory cycle: volume V, flow $\dot{V}$, and acceleration $\ddot{V}$ defined as:

$$\dot{V} = \frac{dV}{dt}, \ddot{V} = \frac{d^2 V}{dt^2}, \tag{1}$$

where the flow $\dot{V}$ [m^3/s] is the first derivative of the air volume [m^3] which passes per unit time, while acceleration $\ddot{V}$ [m/s^2] is the second derivative of volume, expressed as the rate of velocity change of air in time.

By applying pressure changes to the opening of the airways, the FOT signal causes the anatomic structures of the human respiratory tract to perform oscillatory motions superimposed over quiet breathing that produces air dynamics defined as flow. The minimum required pressure applied P_{appl}, necessary for the respiration motion, is expressed with Rohrer's respiratory system equation of motion [6], such as:

$$P_{appl} = P_{el} + P_{res} + P_{in} = E_{rs}V + R_{res}\dot{V} + I_{rs}\ddot{V}, \tag{2}$$

with specific pressure characteristics needed to change V, $\dot{V}$, and $\ddot{V}$. Consequently, three coefficients are described to constitute elastic P_{el}, resistive P_{res} and inertia P_{in} pressure: respiratory system elastance ($E_{rs} = P_{el}/V$) [$\frac{Pa}{m^3}$], respiratory system resistance ($R_{rs} = P_{res}/\dot{V}$) [$\frac{Pa}{m^3/s}$], and respiratory system inertial coefficient ($I_{rs} = P_{in}/\ddot{V}$) [$\frac{Pa}{m/s^2}$].

Having the measured data described by the multisine input signal (U_g [kPa]) on the breathing signal of the patient, we extract the information from the measured pressure (P_{appl}) and flow ($\dot{V}$) signals over a predefined period of time.

The ratio of the Fourier transforms from pressure P and flow $\dot{V}$ gives the respiratory impedance Z_{rs}, defined as the total load imposed against the respiratory system motion [6]. Furthermore, the outcome respiratory impedance Z_{rs} has been identified as the ratio between the cross-power spectra of input (U_g) – output

$(P, \dot{V})$ signals, using electrical analogy models. Through the spectral analysis we obtain the frequency response of the system given by [24], [35]:

$$Z_{rs}(j\omega) = \frac{S_{PU_g}(j\omega)}{S_{\dot{V}U_g}(j\omega)} \tag{3}$$

when considering $\omega = 2\pi f$ the angular frequency [rad/s], with f the selected oscillations frequencies [Hz] in U_g signal.

Respiratory impedance can be defined in the Cartesian complex form, considering the elastic and inertial forces, together with the system resistance:

$$Z_{rs}(j\omega) = R_{rs} + jX_{rs} = R_{rs} + j\left(\omega I_{rs} - \frac{1}{\omega C_{rs}}\right), \tag{4}$$

where $j = \sqrt{-1}$ is the imaginary number, R_{rs} the respiratory resistance (real part), X_{rs} the respiratory reactance (imaginary part), C_{rs} the respiratory compliance ($E_{rs} = 1/C_{rs}$).

R_{rs} reflects opposition to pressures changes in $\dot{V}$, while for the X_{rs} the pressures are in phase with V changes. The frequency where the reactance (X_{rs}) is equal to 0 ($Z_{rs} = R_{rs}$) is called resonant frequency (F_{res}) (i.e., mechanical-electrical inertance and elastance contributions are equal).

D. Parametric Model for Respiratory Impedance

An electrical circuit model analogous to the respiratory system allows the characterization of respiratory impedance Z_{rs} through three circuit elements: a resistor with total respiratory system resistance R_{rs} $[\frac{kPa}{l/s}]$ (by replacing the electric current i with flow $\dot{V}$), an inductor with total respiratory system inertance L_{rs} $[\frac{kPa}{l/s^2}]$ and a capacitor with total respiratory system compliance C_{rs} $[\frac{l}{kPa}]$ [20]. As already shown in [24], the respiratory impedance is best modeled as follows:

$$Z_{rs}(s) = R_{rs} + L_{rs}s^{\alpha_{rs}} + \frac{1}{C_{rs}s^{\beta_{rs}}}, \tag{5}$$

with s the Laplace operator, and fractional orders are defined as $\alpha_{rs}, \beta_{rs} \in (0, 1)$. This FOIM model has been linked to mechanical and physiological lung function [20], [24].

For identification, we used MATLAB , MathWorks, Optimization Toolbox with `lsqnonlin` function for finding parameters that minimize the error while satisfying the constraints. Using the non-linear least-squares identification algorithm, we estimated the five model parameters by successive iterations. Every iteration provides an approximate solution to the model parameters by minimizing the sum of squares of residual errors. Based on the pathophysiology link between obstructive diseases (COPD) and cancer, the initial values for the search optimization have been adjusted with originating values from previously reported literature studies for obstructive diseases [24]. These parameters have been used as parent values in MATLAB, MathWorks, Global Optimization Toolbox, for a genetic algorithm. The `ga` function creates a random initial vector of parameters, optimized successively for 10.000 random iterations until the end conditions are met.

Another approach for accounting the tissue mechanics is defining the impedance by two free parameters, G_r and H_r

[22], [24], [36]. G_r is commonly called tissue damping and is related to tissue resistance, founding the dissipative component of the impedance, while H_r characterizes the elastic energy storage within the lung tissues. Hence, the input impedance of the constant phase model of the lung becomes [21]:

$$Z(\omega) = R_{rs} + L_{rs}j\omega^{\alpha_{rs}} + \frac{G_r - jH_r}{\omega^{\beta_{rs}}}, \tag{6}$$

with G_r and H_r represented using the definition of complex numbers for (6) [26]:

$$G_r = \frac{1}{C_{rs}\omega^{\beta_{rs}}} \cos\left(\beta_{rs}\frac{\pi}{2}\right) \tag{7}$$

$$H_r = \frac{1}{C_{rs}\omega^{\beta_{rs}}} \sin\left(\beta_{rs}\frac{\pi}{2}\right) \tag{8}$$

We acknowledge that the presence of heterogeneity within the constant phase model arises from the G_r/H_r ratio, termed hysteresivity η_r [22], [36]:

$$\eta_r = \frac{G_r}{H_r} \tag{9}$$

Literature studies have shown that η_r increases progressively with the degree of heterogeneity present in the lung tissue and therefore is an indicator of heterogeneity [10], [37].

The constant phase model from (6) assumes that the lung is ventilated homogeneously. Hence, the observation is that η_r always seems to increase during airways obstruction and with severity. When determining Z_{rs} in spontaneously breathing, the tissue heterogeneity is best characterized at lower frequencies, similar to the frequency of breathing and its harmonics. The reason is that as frequencies decrease below 5 Hz, we can observe a high increase in resistance while reactance is decreasing. Hence, the mechanical properties described by resistance (i.e. stiffness/elastance) are increased in high tissue heterogeneity, being very sensitive to frequency.

In contrast, the index of heterogeneity of the obstruction within the lungs assessed with Resmon PRO device is given by the R_{5-19} parameter which reflects the resistance in the small airways. It is defined as the difference between resistance at 5 Hz R_5 (total airway resistance) and 19 Hz R_{19} (resistance of the large airways). Consequently, patients with mixed obstructive and restrictive diseases tend to have greater values for R_{5-19}. Likewise, in lung cancer, this parameter is expected to reflect higher heterogeneous ventilatory mechanics [19].

E. Non-Linearities Detection and Heterogeneity

Respiratory tissue with pathology is heterogeneous and implies a non-linear dynamic response when challenged through lung function tests. When measured at the mouth of the patient, during tidal breathing, interference occurs between the excitatory signal $U_g(t)$ and the breathing signal $b(t)$. For Resmon PRO device, this interference is avoided by the selection of excitatory frequencies a decade higher than breathing frequency (≈ 0.3 Hz). However, in 4P-FOT, a direct non-linear dynamic interaction takes place between the breathing patient and the device. For the evaluation of the non-linear distortions provoked by the generator alone, an identification method has been applied.

Best Linear Approximation (BLA) is extracted from the data with algebraic calculations between the input and the output signals to correct the final result in measured patients [38]. BLA of a non-linear system requires the minimization of the mean squared error. This method has been described thoroughly for 4P-FOT in [10] and only the core principles are given here.

The designed excitation signal is fed seven consecutive times to the device and stimulates the non-linear interactions among all the frequency components. After excitation, the output will contain frequency contributions with $f_i \pm f_j$ even (quadratic) and $f_i \pm f_j \pm f_k$ odd (cubic) non-linearities. As all the frequencies in the excitation signal are odd multiples of the fundamental harmonic their contribution in response to the system is different depending on the non-linearity being even or odd. Moreover, the system was excited with only odd harmonics in the multisine signal, avoiding the presence of even non-linear distortions at the excited frequencies. This excitation allows separating the disturbing noise influence from the non-linear contributions existing in the respiratory system, defined in [24] by T index:

$$T_{index} = \frac{\sum |P_{even}| + \sum |P_{odd}|}{\sum |P_{exc}|} \bigg/ \frac{\sum |U_{even}| + \sum |U_{odd}|}{\sum |U_{exc}|} \tag{10}$$

where T index represents the ratio between the contributions at all non-excited frequencies with respect to the contributions at the odd excited frequencies. We calculate the sum of the absolute values of all the contributions in both the pressure and input flow signals, at excited (odd) and non-excited (even, odd) frequencies.

Another approach is to make use of averaging modified periodograms. The concept applied refers to reducing the non-linear effect over the frequency response function. The presence of measurement non-linearities in the process implies the averaging of estimated samples to minimize the effects of noise variance on our output estimates. We averaged over several frequency components, at the cost of reducing the frequency resolution, and noise, respectively. The method consists of a number of samples N divided into sub-intervals p with length L. So if we average over p-frequency components we have that the resolution bandwidth becomes $B_e = \frac{p}{NT_s}$, with sampling time T_s. Increased chosen values of L similar to N provoke higher resolution, while decreased L signifies lower resolution, but also reduced noise. Usually, the noise is introduced by the breathing frequency harmonics.

F. Statistical Analysis

Statistical analysis was performed using MATLAB, MathWorks, Statistics and Machine Learning Toolbox to describe, analyze, and model the data. The results were tested and plotted using the one-way analysis of variance (ANOVA) and compared between measurement groups using boxplots. By contrast, Kruskal–Wallis test did not assume a normal distribution of the subjects, unlike ANOVA. The results with p-values < 0.05 were considered statistically significant. Statistical analysis was performed on tissue heterogeneity using G_r, H_r, η_r, as well as T index and R_{5-19} index.

TABLE III
BREATHING PATTERN PARAMETERS REPORTED BY RESMON PRO

	Measurement #1	Measurement #2	Measurement #3
T_i [s]	1.737	1.788	1.786
T_e [s]	2.534	2.545	2.609
T_i/T_{tot}	0.434	0.437	0.434
RR [bpm]	16.507	16.475	16.846
V_t [l]	1.133	1.132	1.090
V_t/T_i [l/s]	0.689	0.692	0.658
V_t/T_e [l/s]	0.481	0.489	0.461
V_e [l/min]	16.032	16.997	16.002
F_{res} [Hz]	18.571	17.908	18.978
F_{res} $Zscore$	1.215	1.025	1.317
F_{res} $pred$ [%]	125.23	137.84	154.84

III. RESULTS

Seventeen patients were included in the final analysis. Age differed numerically across patients with a median age of 66 years for male patients and 73 years for women. Statistically significant differences were seen between patients for the body mass index (BMI), with a higher prevalence of respiratory disorders in patients with BMI over 25. As reported in Table I, nine patients suffer from other respiratory diseases with different levels of severity, concomitant with lung cancer.

Table III shows the Resmon PRO device results of the breathing pattern parameters calculated based on all accepted breaths of the test, with an accuracy of 10% [34]. We found significant differences only for T_i/T_{tot}, respiratory rate, and minute ventilation (p-values$\ll$0.0005) between the measurements for each patient. In contrast, using one-way ANOVA for the three groups of measurements, a p-value=0.9207 shows no difference for the resonant frequency acquired with Resmon.

A. Identification

The results are presented for two different frequency intervals according to each measuring FOT device: (i) low-range frequencies between 0.2–2 Hz (4P-FOT) and (ii) high-range frequencies between 5–37 Hz (Resmon PRO).

1) Data Processing: The frequency response has been derived from raw data measurements using (3) by means of spectral analysis. The results are plotted as frequency-dependent complex impedance consisting of resistance (real part) and reactance (imaginary part). In terms of the frequency content of the signals, the boxplots in Figs. 3 and 4 display the distribution of impedance data for all patients per corresponding frequency and measurement. It is unsure that the 4P-FOT device can capture the real part of the impedance at low frequencies where slightly negative values of the resistance can be depicted.

Although the obtained data of the lung cancer patients compared to the healthy impedance data is observed to have higher respiratory resistance varying negatively with frequency, and lower respiratory reactance frequency-dependent [33], the sensitiveness of the devices is further reflected in the actual values of the impedance components. Measurements at high-frequency oscillations show a resistance significantly increased compared to the one measured at low-frequency oscillations becoming more negative compared to reactance in 4P-FOT.
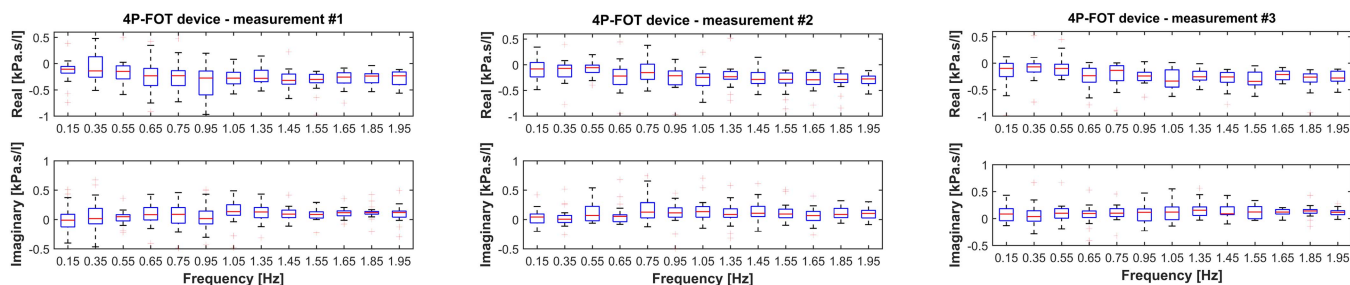
Fig. 3. 4P-FOT at low frequencies – Non-parametric respiratory impedance Z_{rs} defined in the frequency domain as the ratio between the cross-power spectra of input (U_g) – output $(P, \dot{V})$ signals. The result is a complex impedance (frequency dependent) with two components: "real part" (resistance, describing the damping tissue properties), and "imaginary part" (reactance, characterizing the elastance tissue properties at low frequencies). The boxplots display the distribution of impedance data per frequency, for all patients.
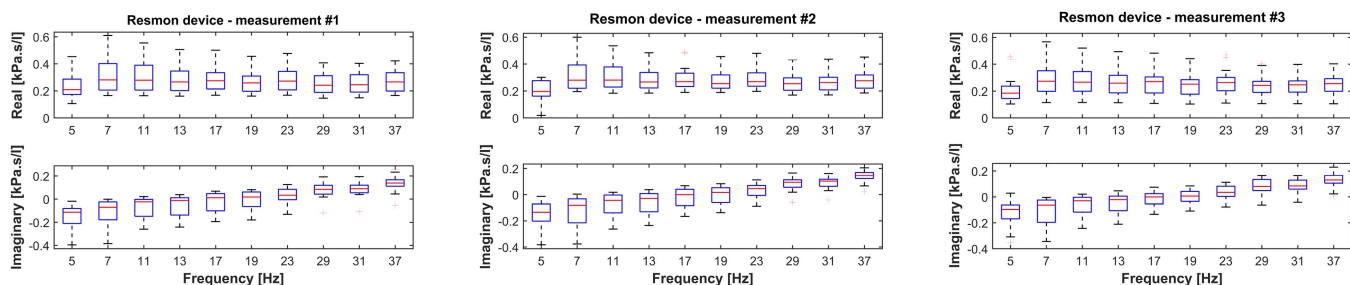
Fig. 4. Resmon PRO at high frequencies – Calculated respiratory impedance Z_{rs} represented by its "real part" (resistance, describing the damping tissue properties), and "imaginary part" (reactance, characterizing the inertance tissue properties (at high frequencies). The boxplots display the distribution of impedance data per frequency, for all patients.
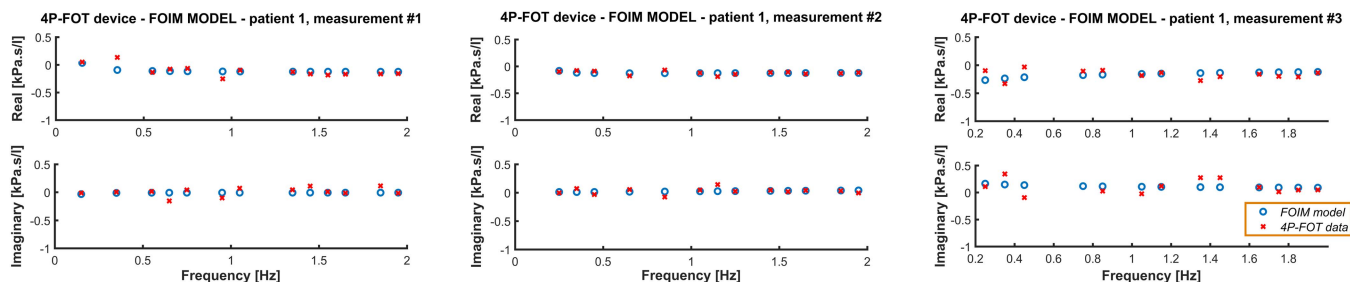

Fig. 5. 4P-FOT at low frequencies – Parametric identification of the respiratory impedance with FOIM model presented (example for one patient).

The reported values in the literature for resonance frequency for healthy adults are between 8–12 Hz [36], for COPD 6–20 Hz [3], [4], while for lung cancer patients measured in this clinical study are 6.92–36.15 Hz. This frequency of applied oscillations is the point where the imaginary part of the impedance crosses zero, depends on the balance between different mechanical properties (elastic, inertial), and expresses that the pressure and flow responses are perfectly in phase. From the reported values in the clinical reports created by Resmon PRO, we obtained an averaged resonant frequency (F_{res} [Hz]) per measurement, as follows: 18,57 Hz measurement #1, 17.9 Hz measurement #2, and 18.97 Hz (measurement #3).

2) Model Parametric Identification: Figs. 5 and 6 show the performance of the FOIM model from (5) in the studied group with both devices. The associated model adjustments fol-

low the characteristics of the measured respiratory impedance, with high-frequency resistance due to restrictive and mixed obstructive/restrictive pathophysiology of the diseased lung. It can be observed that the model characterizes well the frequency-dependent behavior of the impedance acquired in lung cancer patients. Table IV presents the impedance data with the corresponding mean and standard deviation values observed in the real and imaginary parts of the adjusted impedance. On examining the parameters obtained with the FOIM model, no significant variability was observed between the three sets of measurements studied.

However, increases in compliance C_{rs} at low-range frequencies and resistance R_{rs} at higher frequencies can be observed also in Figs. 7 and 8. The figures show the results tested using the one-way analysis of variance. Consequently, among the Resmon
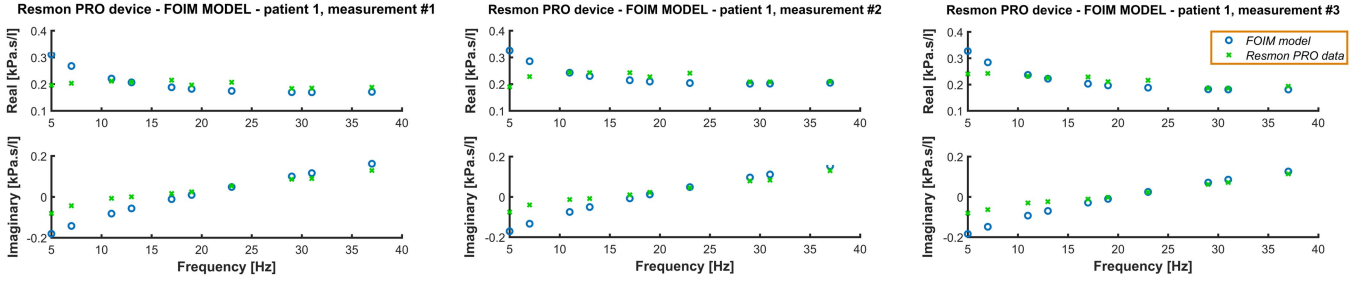
Fig. 6. Resmon PRO FOT at high frequencies – Parametric identification of the respiratory impedance with FOIM model presented (representation of fitting example for the same patient data as used in Fig. 5).
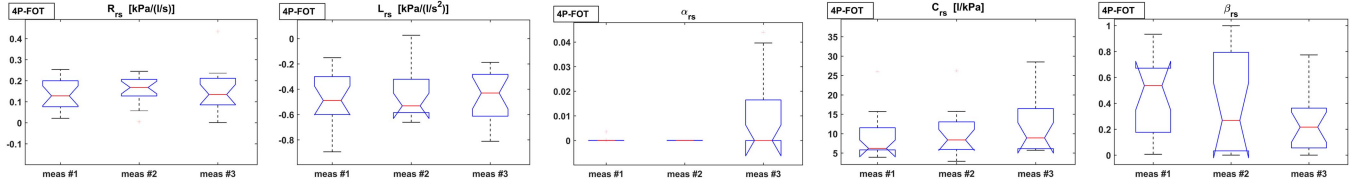

Fig. 7. Representation of FOIM model parameters values for all three measurements obtained with 4P-FOT device at low frequencies. The p-values returned by one-way Anova are: R_{rs} - 0.318, L_{rs} - 0.349, α_{rs} - 0.315, $C_r s$ - 0.744 and β_{rs} - 0.123.
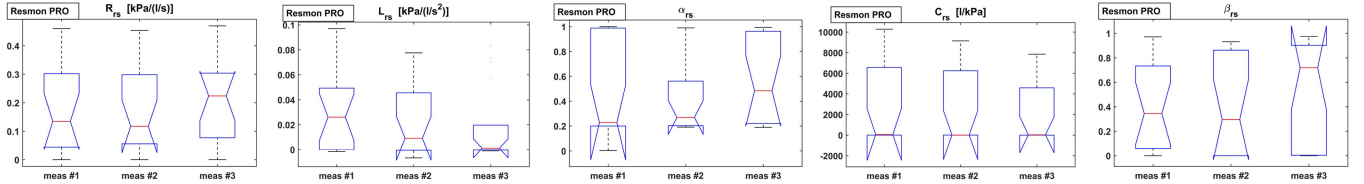

Fig. 8. Representation of FOIM model parameters values for all three measurements obtained with Resmon PRO device at high frequencies. The p-values returned by one-way Anova are: R_{rs} - 0.787, L_{rs} - 0.518, α_{rs} - 0.39, C_{rs} - 0.815 and β_{rs} - 0.338.

TABLE IV
MEAN (STANDARD DEVIATION) IDENTIFIED VALUES FOR THE FOIM MODEL PARAMETERS

Device	Meas.	R_{rs}	L_{rs}	α_{rs}	C_{rs}	β_{rs}
4P-FOT at low frequencies	#1	0.158 (0.1067)	-0.5205 (0.1243)	0.0046 (0.0127)	-146.3078 (692.7092)	0.3945 (0.3157)
	#2	0.5604 (1.6894)	-0.8479 (1.6791)	0.0508 (0.1628)	25.8149 (59.4857)	0.3873 (0.3718)
	#3	1.1117 (2.7410)	-1.4017 (2.7731)	0.0186 (0.0419)	44.3010 (133.6014)	0.2453 (0.2396)
Resmon PRO at high frequencies	#1	0.1709 (0.1411)	0.0307 (0.0324)	0.4562 (0.3953)	29761.37 (37950.85)	0.3931 (0.3475)
	#2	0.1729 (0.1509)	0.0225 (0.0261)	0.4263 (0.3212)	25220.51 (36717)	0.3839 (0.4014)
	#3	0.2070 (0.1472)	0.0178 (0.0309)	0.6001 (0.3608)	20139.9 (29373.79)	0.5646 (0.4016)

Values are given as mean, while values in brackets denote the standard deviations.

data, inertance L_{rs} and compliance C_{rs} showed significant decreases, while the fractional parameter β_{rs} has an increase from the first measurement to the third (as depicted in Fig. 8).

B. Characterization of the Tissue Heterogeneity

1) Tissue Heterogeneity: The results are represented through their physiological meaning using the damping (G_r), elastance (H_r), and hysteresivity coefficient (η_r) values from

(7), (8), and (9). Hysteresivity describes the heterogeneity of the lung, with greater values associated with increased heterogeneity in the affected tissue by tumor occurrence. In Figs. 9 and 10 are depicted the damping associated with energy dissipation in the respiratory system, the elastance reflecting the potential elastic energy storage and their ratio which decreases with the applied treatment due to the changes in pulmonary structure (i.e., tumor minimization or elimination). Throughout the measurements, increased values were found for G_r along with a reduction in H_r as shown in Fig. 9.

The quantification of heterogeneity of the obstruction within the lungs is characterized by R_{5-19} index for Resmon PRO device. In Fig. 11 is represented the difference between resistance at 5 Hz and 19 Hz for all patients, with the observation that the resistance in small airways due to obstruction caused by the tumor is decreasing in the cases where the treatment was effective. However, if this index increases compared with the first measurement, it can indicate an inflammation of the tissue caused by the applied radiation, with later effects in toxicity of the initial surrounding tissue of the tumor.

2) Non-Linearities Detection With 4P-FOT: As expected, noise is detected in the measurements, but coincides with the breathing frequency and harmonics of the patient. For example, in Fig. 12 the breathing frequency of the patient is 0.15 Hz. The
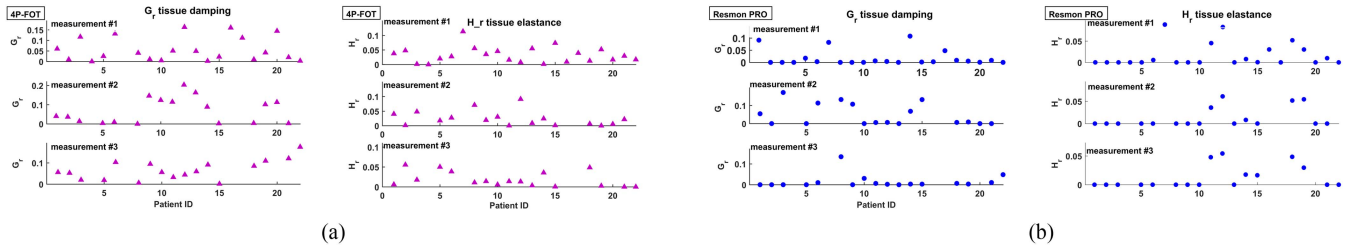
Fig. 9. Tissue damping and tissue elastance, characterized by G_r, H_r in patients with lung cancer, assessed with (a) 4P-FOT device and (b) Resmon PRO device.
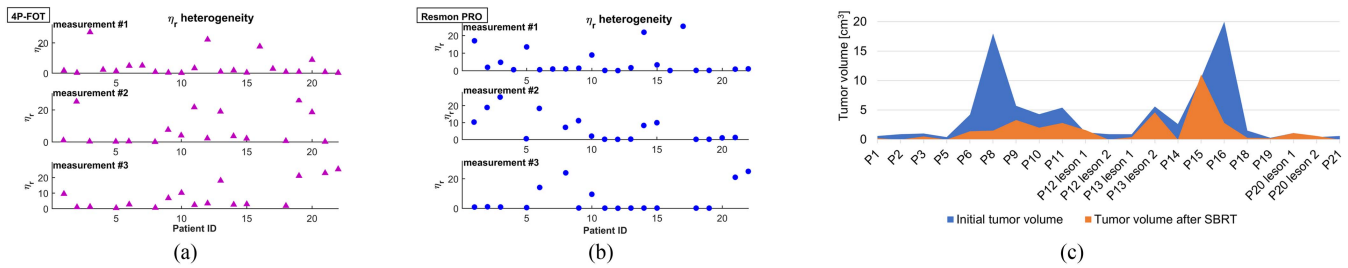

Fig. 10. Tissue heterogeneity characterized by η_r in patients with lung cancer, assessed with (a) 4P-FOT device and (b) Resmon PRO device; (c) Tumor volume measurements from CT scans at the time of FOT measurement #1 (initial tumor volume) and FOT measurement #3 (tumor volume after approx. 3 months of SBRT treatment).
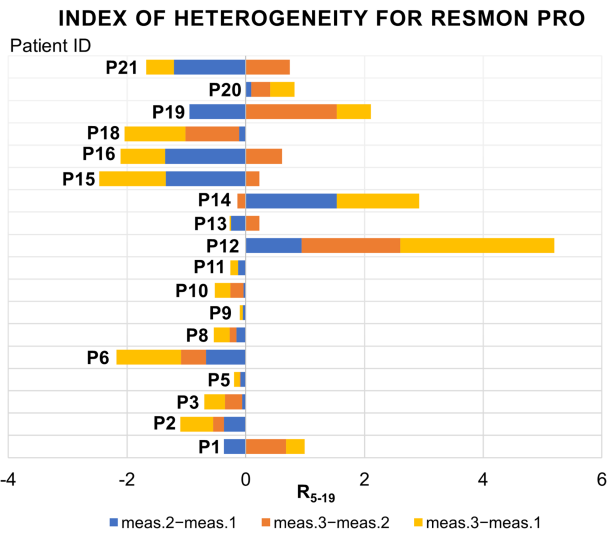

Fig. 11. Index of heterogeneity for Resmon PRO - difference between the values of R_{5-19} for measurement #2–measurement #1, measurement #3–measurement #2, and measurement #3–measurement #1.

harmonics, defined as multiples of this fundamental frequency will be also affected and presents noise, as shown in the figure. However, those harmonics become small in amplitude as the frequency increases, such that the estimation of the impedance using explained methods poses no problem.

A method for quantifying the non-linear effects coming from the airways and lung tissue at lower frequencies is introduced for validating the hypothesis that T index is increased in patients diagnosed with respiratory diseases. By contrast, after radiation is applied, tissue is more likely to suffer from its exposure, needing more time to heal. Therefore, Fig. 13 shows a progressive increase in the median T index with measurements. Even if the values for the measurement #1 are similar to the non-linear distortions in the COPD groups [24], the second and third measurements after treatment is applied express higher values than the other reported data (as seen in Fig. 13 where values approach 2).

In Fig. 14, an example of even and odd harmonics identification using the method given in [35] is shown and described in detail in [15]. The method consists of a number of samples ($N=120000$) divided into sub-intervals ($p=7$) with length ($L=20000$), and frequency resolution bandwidth $B_e=0.05$ Hz) [38]. Fig. 14 depicts a schematic of the measurements non-linearities and the corresponding output.

IV. DISCUSSION

Complementary tools to better treat NCSCLC patients have considerable value for clinical treatment management. Although the optimal treatment strategy for an individual patient depends on the size and location of the tumor, the FOT results can give complementary information about the mechanical properties and tissue heterogeneity of the lung. This study was undertaken to investigate if FOT-derived parameters are potential indicators of pulmonary health status and could predict lung tissue changes in advanced NSCLC.

The current study demonstrated for the first time that characterization of respiratory impedance may be helpful in the
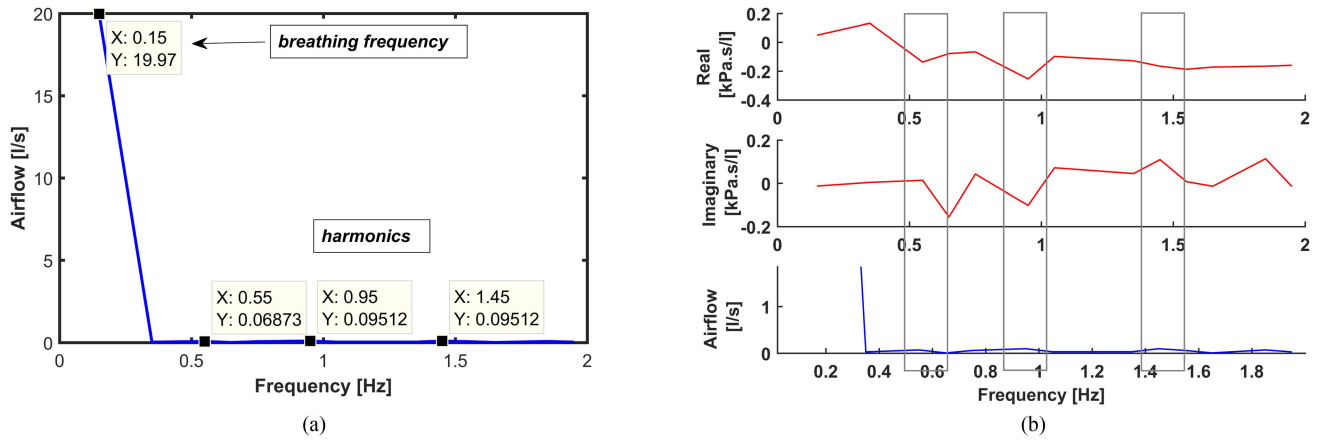
Fig. 12. (a) Representation of the breathing frequency and its harmonics; (b) The breathing frequency introduces noise in the output signal measured (airflow).
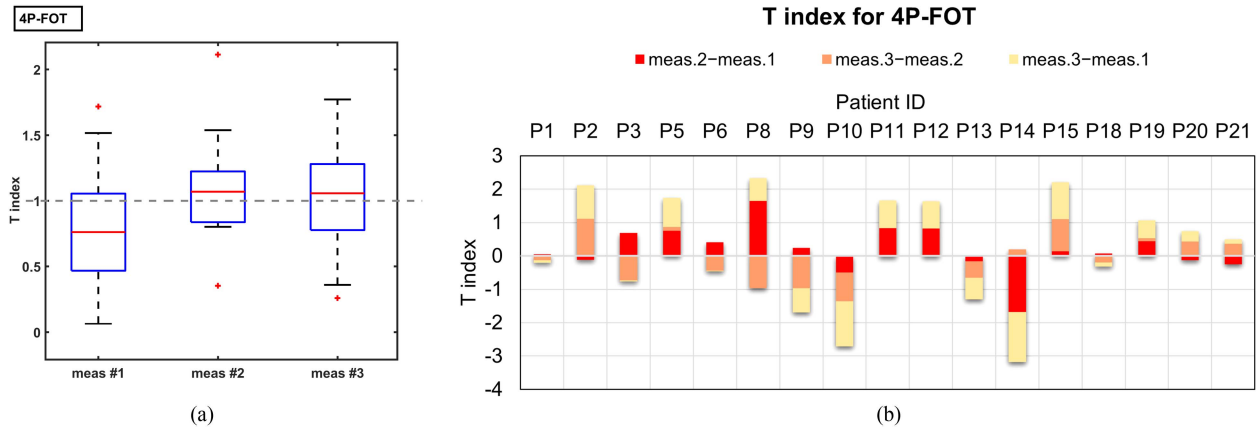

Fig. 13. T index representation for 4P-FOT device at lower frequencies. (a) Boxplot for T index in NSCLC patients, grouped per sets of measurements; (b) Anova difference between the values of T index for measurement #2–measurement #1, measurement #3–measurement #2, and measurement #3–measurement #1.
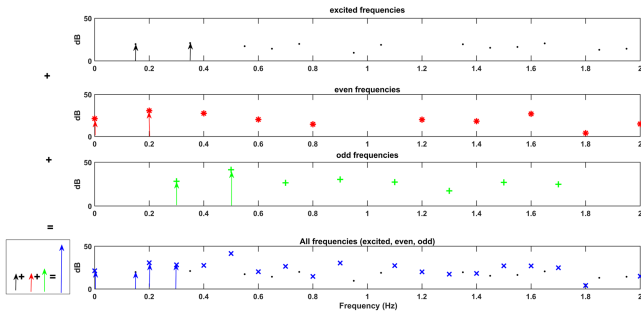

Fig. 14. Schematic representation of the non-linear contributions, divided into excited, even, and odd frequencies.

prospective assessment of lung function; i.e., through evaluation of respiratory impedance, respiratory mechanics, tissue properties, and tissue heterogeneity. The impedance is determined by measuring the pressure and the airflow, parameters that vary in different conditions of the respiratory system. From the pathological viewpoint, the tumor will invade the healthy lung tissue

which will automatically lead to obstructions and blockages in the respiratory branches, modifying the respiratory function.

This study brings evidence regarding the relevance of evaluating respiratory impedance in lung cancer patients. The identified values for the complex respiratory impedance Z_{rs} as depicted in Figs. 3 and 4, reveal that:

- R_{rs} increases significantly in lower frequencies and decreases as frequency increase, suggesting local airway obstruction, most likely due to tumor fibrosis accumulation.
- X_{rs} becomes significantly more negative indicating greater elastance or stiffness.

Our observations for lung cancer patients are in agreement with other studies which demonstrated that adult patients with obstructive airway diseases have increased R_{rs} and more negative X_{rs} values [6], [10]. Several factors provoke a slightly increase of the mean value of R_{rs} and f_{res} at frequencies $< 5\,\mathrm{Hz}$ (peripheral airways), and lower at higher frequencies, such as the aging of the respiratory system for the elderly subjects, or the reduction of lung volume when the elastic pressure tends to reduce the airways diameter. Likewise, due to hyperinflation, periphery

non-homogeneity and flow limitation, the resistance induces a lack of sensitivity, while the chest wall and tissue compliance decrease, causing increased capacitance. Therefore, the results suggest a higher accuracy of pathological values for reactance than resistance in higher degrees of airway obstruction.

The current study found that airway alterations in lung cancer are similar with the modifications of respiratory impedance and its components occurred in other obstructive respiratory diseases (e.g., COPD). To date, diseases with restrictive and mixed (obstructive/restrictive) pathophysiology were proven to demonstrate an almost identical behavior to the one expressed in peripheral airways obstruction [6]. Usually, the obstruction in lung cancer is situated peripherally in the bronchial tree, where the medium and small size bronchi are not supported by cartilage. All of the changes produced in lung cancer by bronchial blocking and obstructive inflammation led to corresponding changes in F_{res}, R_5, R_{20}, and X_5 between the measurements acquired with Resmon PRO.

The increased hysteresivity coefficient η_r signifies increased inhomogeneities and structural changes in the alveolar walls towards wall destruction [37]. Since the parameter embodies capacitor properties, it characterizes alterations in the lung compliances across the airway tree. Increasing heterogeneity decreases the effective reactance (i.e., increases stiffness/elastance) at any given frequency in obstructive airways diseases. Other parameters introduced in literature, such as T index [24] and R_{5-19} [34] are also capturing successfully the heterogeneity changes in lung cancer tissue after treatment.

To visually characterize heterogeneity in lung cancer, a CT scan is useful. However, among patients with lung cancer treated with SBRT, it is not recommended to perform multiple CT scans in a short period of time due to constant radiation exposure. To avoid over-radiation, a CT scan dose reduction is applied, but it results in reduced imaging resolution for detecting obstructions in the peripheral airways and early onset of lung stiffening. In this context, FOT devices are extremely useful to first asses the functional damage and characterize lung obstruction in these frail patients, at any time and avoid additional maneuvers [39]. Another advantage of FOT over standardized PFTs is its sensitivity to detect peripheral airway obstructions, depending on the range of frequency applied to the respiratory system (closer to the breathing frequency ~ 2 Hz, or higher until 37 Hz) [40].

Effective radiotherapy can be endorsed by the use of FOT to compare the lung function before and after treatment, when the tumor decreases, leading to the improvement in airway obstruction and compression while decreasing resistance in peripheral airways. Each patient develops special characteristics in tumor size and sensitivity evolution, requiring personalized treatment with a focus on adjacent solutions. For example, changes in FOT results may be used as surrogate parameters to assess treatment efficacy, especially if it could guide the radiation treatment management [19].

Clinicians already emphasized the risk for patients that develop radiation-induced toxicity, despite obtaining good results with SBRT and improved treatment strategies. Although scarce, studies report that poor lung function assessed in patients before RT may suggest a high probability of toxicity after RT, compared to patients that initially had a better lung function [41]. Although

FOT data is not enough for outcome prediction, we believe the results of our study suggest that fusing imaging tools, functional and mathematical parameters provide potentially important information for predicting the risk of radiation pneumonitis. In our study, five patients have been reported to have the lesion not measurable anymore (no nodule detectable), but surrounded by a large area of radiation pneumonitis at the follow-up visit when a second CT scan was performed. This is the first use of FOT potential in this problem. We acknowledge that further research is needed to identify and prospectively assess predictors of treatment outcomes and RT-induced lung injury.

Despite the high relevance of the observations extracted from this study, some limitations can be enumerated. Firstly, the clinical trial consists of a small subject database, this being a proof-of-concept study and providing first-hand evidence of FOT use in lung cancer patients. Secondly, a universal categorization of the patients could not be defined to allow the grouping of a more detailed correlation between cancer tissue evolution and respiratory mechanics. Thirdly, the occurrence of patients with NSCLC treated with SBRT represents a narrow group of patients. This requires extensive study time, while the present study execution is approximately 12 months for 22 patients. Additionally, the high burden of other comorbidities that could have affected the respiratory function was not considered (e.g., COVID-19). Finally, a comparison of multiple tests for the same patient was not possible to be acquired in the same session due to the frailty of some patients.

This study encountered considerable practical difficulties in performing the measurements on patients in the clinical environment. Several efforts were made to overcome the following issues emerging from conducting this long-term study: a limited number of patients treated specifically with SBRT, sparse patients in the time-span of the study, several drop-outs between the three measurements due to patient's absence or disease progression, ensuring close coordination among physicists, technicians, and clinicians, compliance of the FOT measurement time with the timing and schedule for RT treatment delivery (according to the availability of specific equipment), reluctantly patient participation in clinical trials, shortages from pandemic causes, etc.

V. Conclusion

This research aimed to examine the use of FOT in lung cancer patients and build the hypothesis that the proposed techniques provide unique insight into the changes in the respiratory function and pathophysiology developed at the appearance of a lung tumor. We performed a proof-of-concept clinical trial for clinical validation of presented research methods in patients with NSCLC. The results of this investigation confirmed that FOIM fitted well the clinical data acquired for respiratory impedance in lung cancer. Nevertheless, there are differences in the lung mechanics and tissue heterogeneity assessed before and after SBRT. This is the first report of FOT as a complementary tool in lung cancer management and provides a basis for the feasibility of this approach in clinical settings. As such, fusion through parameterisation of multiple information sources (e.g., lung function tests, tumor volume scans) is further envisaged.

References

[1] L. Torre-Bouscoulet et al., "Longitudinal evaluation of lung function in patients with advanced non-small cell lung cancer treated with concurrent chemoradiation therapy," *Int. J. Radiat. Oncol. Biol. Phys.*, vol. 101, no. 4, pp. 910–918, Jul. 2018.

[2] D. S. Ettinger et al., "Non-small cell lung cancer, version 3.2022, NCCN clinical practice guidelines in oncology," *J. Natl. Compr. Canc. Netw.*, vol. 20, no. 5, pp. 497–530, May 2022.

[3] E. Oostveen et al., "Respiratory impedance in healthy subjects: Baseline values and bronchodilator response," *Eur. Respir. J.*, vol. 42, pp. 1513–1523, Dec. 2013.

[4] O. Kalchiem-Dekel and S. E. Hines, "Forty years of reference values for respiratory system impedance in adults: 1977–2017," *Respir. Med.*, vol. 136, pp. 37–47, Mar. 2018.

[5] G. G. King et al., "Technical standards for respiratory oscillometry," *Eur. Respir. J.*, vol. 55, Feb. 2020, Art. no. 1900753.

[6] A. S. Lappas et al., "Forced oscillations in applied respiratory physiology: Clinical applications," *Clin. Res. Pulmonol*, vol. 2, no. 2, Apr. 2014, Art. no. 1016.

[7] P. Bhattarai et al., "Clinical application of forced oscillation technique (FOT) in early detection of airway changes in smokers," *J. Clin. Med.*, vol. 9, no. 9, Aug. 2020, Art. no. 2778.

[8] I. Assadi et al., "Evaluation of respiratory properties by means of fractional order models," *Biomed. Signal Process. Control*, vol. 34, pp. 206–213, Apr. 2017.

[9] J. K. Lui et al., "The role of heterogeneity in asthma: A structure-to-function perspective," *Clin. Trans. Med.*, vol. 6, no. 1, pp. 1–11, 2017.

[10] M. Ghita et al., "Low frequency forced oscillation lung function test can distinguish dynamic tissue non-linearity in COPD patients," *Front. Physiol.*, vol. 10, Nov. 2019, Art. no. 1390.

[11] C. O. Ribeiro et al., "Oscillation mechanics, integer and fractional respiratory modeling in COPD: Effect of obstruction severity," *Int. J. Chronic Obstructive Pulmonary Dis.*, vol. 15, pp. 3273–3289, Dec. 2020.

[12] D. Blanco-Almazán et al., "Combining bioimpedance and myographic signals for the assessment of COPD during loaded breathing," *IEEE Trans. Biomed. Eng.*, vol. 68, no. 1, pp. 298–307, Jan. 2021.

[13] D. Copot et al., "Structural changes in the COPD lung and related heterogeneity," *PLoS One*, vol. 12, no. 5, May 2017, Art. no. e0177969.

[14] C. M. Ionescu et al., "Mechanical properties of the respiratory system derived from morphologic insight," *IEEE Trans. Biomed. Eng.*, vol. 56, no. 4, pp. 949–959, Apr. 2009.

[15] C. M. Ionescu et al., "Respiratory mechanics in children with cystic fibrosis," *Biomed. Signal Process. Control*, vol. 11, pp. 74–79, 2014.

[16] C. M. Ionescu, E. Derom, and R. De Keyser, "Modelling respiratory impedance in patients with kyphoscoliosis," *Biomed. Signal Process. Control*, vol. 11, pp. 36–41, May 2014.

[17] R. Sokai et al., "Respiratory mechanics measured by forced oscillation technique in rheumatoid arthritis-related pulmonary abnormalities frequency-dependence, heterogeneity and effects of smoking," *SpringerPlus*, vol. 5, pp. 1–12, Mar. 2016.

[18] H. H. Alamdari et al., "High frequency-low amplitude oscillometry: Continuous unobtrusive monitoring of respiratory function on PAP machines," *IEEE Trans. Biomed. Eng.*, vol. 69, no. 7, pp. 2202–2211, Jul. 2022.

[19] S. Nakano et al., "Perioperative evaluation of respiratory impedance using the forced oscillation technique: A prospective observational study," *BMC Anesthesiology*, vol. 16, no. 1, pp. 1–8, Jul. 2016.

[20] C. M. Ionescu, *Lung Function Testing in the 21st Century: Methodologies and Tools Bridging Engineering to Clinical Practice*, 1st ed. London, U.K.: Elsevier, 2019.

[21] H. H. Alamdari, K. El-Sankary, and G. N. Maksym, "Time-varying respiratory mechanics as a novel mechanism behind frequency dependence of impedance: A modeling approach," *IEEE Trans. Biomed. Eng.*, vol. 66, no. 9, pp. 2433–2446, Sep. 2019.

[22] J. H. T. Bates, *Lung Mechanics: An Inverse Modeling Approach*, New York, NY, USA: Cambridge Univ. Press, 2009.

[23] J. H. T. Bates et al., "Altered airway mechanics in the context of obesity and asthma," *J. Appl. Physiol.*, vol. 130, no. 1, pp. 36–47, Oct. 2020.

[24] C. M. Ionescu, *The Human Respiratory System: An Analysis of the Interplay Between Anatomy, Structure, Breathing and Fractal Dynamics* (BioEngineering Series), London, U.K.: Springer, 2013.

[25] D. S. Karbing et al., "What is new in respiratory monitoring?," *J. Clin. Monit. Comput.*, vol. 36, no. 3, pp. 599–607, May 2022.

[26] C. Ionescu and J. F. Kelly, "Fractional calculus for respiratory mechanics: Power law impedance, viscoelasticity, and tissue heterogeneity," *Chaos Solitons Fractals*, vol. 102, pp. 433–440, Sep. 2017.

[27] C. Ionescu et al., "The role of fractional calculus in modeling biological phenomena: A review," *Commun. Nonlinear Sci. Numer. Simul.*, vol. 51, pp. 141–159, Oct. 2017.

[28] M. Ghita et al., "Lung cancer dynamics using fractional order impedance modeling on a mimicked lung tumor setup," *J. Adv. Res.*, vol. 32, pp. 61–71, Sep. 2021.

[29] M. Joiner and A. van der Kogel, *Basic Clinical Radiobiology*, 4th ed. London, U.K.: Hodder Arnold, 2009.

[30] C. M. Ionescu et al., "Motion compensation for robotic lung tumour radiotherapy in remote locations: A personalised medicine approach," *Acta Astronautica*, vol. 132, pp. 59–66, Mar. 2017.

[31] M. Ghita et al., "Model calibration of pharmacokinetic-pharmacodynamic lung tumour dynamics for anticancer therapies," *J. Clin. Med.*, vol. 11, no. 4, Feb. 2022, Art. no. 1006.

[32] C. M. Ionescu et al., "Measuring nonlinear effects in respiratory mechanics: A proof of concept for prototype device and method," *IEEE Trans. Instrum. Meas.*, vol. 63, no. 1, pp. 124–134, Jan. 2014.

[33] O. Olarte et al., "Fan-based device for non-invasive measurement of respiratory impedance: Identification, calibration and analysis," *Biomed. Signal Process. Control*, vol. 30, pp. 127–133, Sep. 2016.

[34] *Instruction Manual Resmon PRO FULL - Device for Assessment of Lung Function*, 20th ed., Restech Srl, Milano, Italy: Restech Srl, Jul. 2019.

[35] J. Schoukens, R. Pintelon, and T. Dobrowiecki, "Linear modelling in the presence of nonlinear distortions," *IEEE Trans. Instrum. Meas.*, vol 51, no. 4, pp. 786–792, Aug. 2002.

[36] D. Stamenović and T. A. Wilson, "Parenchymal stability," *J. Appl. Physiol.*, vol. 73, no. 2, pp. 596–602, Aug. 1992.

[37] D. W. Kaczka et al., "Oscillation mechanics of the respiratory system: Applications to lung disease," *Crit. Rev. Biomed. Eng.*, vol. 39, no. 4, pp. 337–359, 2011.

[38] C. Ionescu, J. Schoukens, and R. De Keyser, "Detecting and analyzing non-linear effects in respiratory impedance measurements," in *Proc. Amer. Control Conf.*, 2011, pp. 5412–5417.

[39] C. Ionescu et al., "Monitoring respiratory impedance by wearable sensor device: Protocol and methodology," *Biomed. Signal Process. Control*, vol. 36, pp. 57–62, 2017.

[40] C. S. Stahr et al., "Quantification of heterogeneity in lung disease with image-based pulmonary function testing," *Sci. Rep.*, vol. 6, Jul. 2016, Art. no. 29438.

[41] Z. Kocak et al., "Prospective assessment of dosimetric/physiologic based models for predicting radiation pneumonitis," *Int. J. Radiat. Oncol. Biol. Phys.*, vol. 67, no. 1, pp. 178–186, Jan. 2007.